Vol. 25(1):89-106 | Ocean and Polar Research | March 2003

Article

Nonlinear Tidal Characteristics along the Uldolmok Waterway off the Southwestern Tip of the Korean Peninsula

Sok Kuh Kang*, Ki Dai Yum, Jae-Kwi So, and Won-Oh Song

Coastal and Harbor Engineering Laboratory, KORDI
Ansan P.O. Box 29, Seoul 425-600, Korea

Abstract : Analyses of tidal observations and a numerical model of the M_2 and M_4 tides in the Uldolmok waterway located at the southwestern tip of the Korean Peninsula are described. This waterway is well known for its strong tidal flows of up to more than 10 knots at the narrowest part of the channel. Harmonic analysis of the observed water level at five tidal stations reveals dramatic changes in the amplitude and phase of the shallow water constituents at the station near the narrowest part, while survey results show a decreasing trend in local mean sea levels toward the narrow section. It was also observed that the amplitudes of semi-diurnal constituents, M_2 and S_2 are diminishing toward the narrowest part of the waterway. Two-dimensional numerical modeling shows that the M_2 energy flux is dominated by the component coming from the eastern boundary. The M_2 energy is inward from both open boundaries and is transported toward the narrow region of the channel, where it is frictionally dissipated or transferred to other constituents due to a strong non-linear advection effect. It is also shown that the M_4 generation is strong around the narrow region, and the abrupt decrease in the M_4 amplitude in the region is due to a cancellation of the locally generated M_4 with the component propagated from open boundaries. The superposition of both propagated and generated M_4 contributions also explains the discontinuity of the M_4 phase lag in the region. The tide-induced residual sea level change and the regeneration effect of the M_2 tide through interaction with M_4 are also examined.

Key words : nonlinear tidal phenomena, M_4 generation, Uldolmok waterway, numerical modeling.

1. Introduction

The Uldolmok waterway is a channel connecting the entrance of the South Sea and the Yellow Sea (Fig. 1). Its width is in the order of 1-2 km, its length is about 15 km, and the water depth is about 15 m. As shown in Fig. 1 and 4, the waterway has a narrow section of about 250 m width. This site is well known for its strong tidal flow and a pre-feasibility study for power generation utilizing these tidal currents was made in 1985-1986 by the Korea Ocean Research and Development Institute (KORDI 1986) and again through recent observation in 2002 (MOMAF 2002) where direct current measurement using ADCP was carried out.

Lagrangian current measurements were carried out in 1985 under the bridge connecting the narrowest section of the channel. The current speed, measured with lagrangian method, in the narrowest section during spring and mean tides was estimated. The maximum spring current speed is about 6 m/s at flood, and 5.7 m/s at ebb, respectively, with 4.2 m/s speed during mean ebb tide. This surface magnitude was approximately verified in recent Eulerian observation using ADCP (MOMAF 2002), from which the surface M_2 and S_2 along-channel component are analysized to be 3.70 m/s and 1.24 m/s, respectively.

About a month-long tide level recording was carried out at 4 stations in 1986 along the channel using two types of self-recorders. For the 3 stations 86T1, 86T3 and 86T4, Aanderaa WLR-5 instruments were used. Stations except for 86T4 (located beyond the study domain) are shown in the subset of Fig. 1. At 86T2, observations were recorded using a EPT-3 gauge on an analogue chart as well as in

*Corresponding author. E-mail : skkang@kordi.re.kr

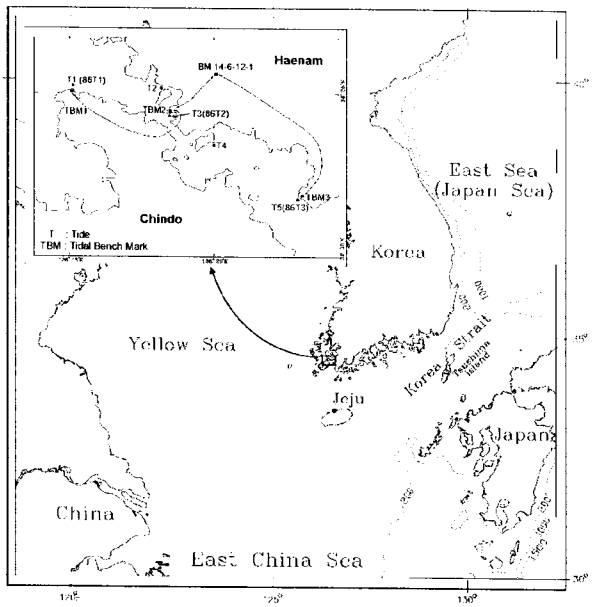

Fig. 1. Location map of tide measurements in 1986 (86T1-86T3) and 1992 (T1-T5) along the Usuyong Waterway between the Chindo and the southwestern tip of the Korean Peninsula. In the subset tidal bench marks (TBM and BM) are indicated as well as the tidal levelling routes according to lines among TBM1, TBM2, BM and TBM3.

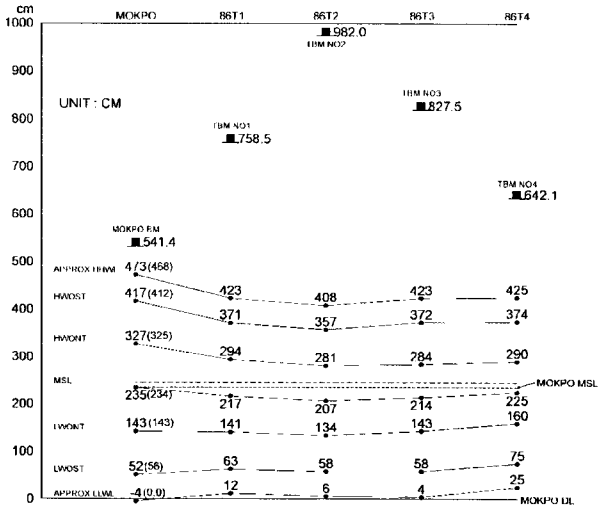

Fig. 2. Elevations of TBMs and various theoretical sea levels.

digital form. During the period of the tide level measurements, tidal staff readings were made for 5 to 7 hours at all three sites during daylight in order to establish the relative tide levels from the four tidal bench marks (TBMs) buried near the tide stations. In order to find the absolute elevations of those TBMs, the BM 14-6-12-1 of the National Geography Institute (NGI) was connected to TBMs No. 1, 2 and 3. The water level recordings were compared with the staff readings and then connected to these land levelling nets. The theoretical sea levels, derived from the harmonic constants as well as mean sea levels, are shown in Fig. 2. The lowest mean sea level is 207 cm at 86T2, while it is 217 cm at 86T1 and 214 cm at 86T3, and gets higher outward from 86T2 station. The sea level set-down is remarkable at 86T2 near the narrowest part of the channel where the strong current occurs.

The results of harmonic analysis for the tidal records in the channel are also described in Table 1. The low value of the M_2 tidal amplitude, as well as the extraordinarily small value of the higher harmonics (M_4 and MS_4), at 86T2, are remarkable. The phase lag of the M_4 constituents at 86T2 shows an abrupt change that cannot be explained by simple wave propagation. As a result of a series of observations related to tides, tidal currents and tidal levelling, it was indicated that there exists some nonlinear phenomena related to higher and lower harmonics generation in association with strong current and large shear of the currents along the channel. However, no thorough analysis was made due to the scarcity of the available data.

Table 1. Tidal harmonic constants for semi, diurnal, quarter-diurnal and fortnight constituents (M_2, K_1, M_4, MS_4) from the analysis of observed data in 1986, along the Uldolmok waterway, Korea. Phase lags in degrees are referred to the local transit time of each tide-generating body. Am and ph denote amplitude and phase lag, respectively. For location of stations, see Fig. 1.

Station	M_2		K_1		M_4		MS_4	
	am cm	ph deg	am cm	ph deg	am cm	ph deg	am cm	ph deg
86T1	115.3	24.6	28.9	244.8	11.5	195.2	7.3	237.8
86T2	111.9	17.9	28.9	243.7	2.2	228.7	2.8	284.5
86T3	114.4	331.2	28.6	219.4	8.1	146.2	5.1	187.6

Therefore, the need for additional measurements and research work were raised to confirm if the observed phenomena is related to actual tidal phenomena.

In this manuscript, the tidal phenomena in the Uldolmok waterway under the influence of a strong current are investigated in terms of additional tidal measurements and two-dimensional tidal modelling. The non-linearity of tidal phenomena in the channel is investigated based upon the analysis of simultaneously measured data at five tidal stations along the channel. Furthermore, the characteristics of the M_2 tide, its energy flux and the non-linear generation of M_4 at the narrowest section are examined using the numerical tidal model. The contributions of both the channel boundary forcing and the local generation effect on the observed features of M_4 are investigated in relation to the abrupt change in the M_4 phase lag in the narrow section. The residual surface or mean sea level in the channel is also investigated using the numerical model and compared with observations. The regeneration of the M_2 by the interaction of M_2 and M_4 is also examined.

2. Measurements and data analyses

To further investigate the characteristics of the shallow water constituents in the Uldolmok waterway, tide level recordings were carried out at 5 stations along the channel during the period of January 15 to February 9-14, 1992. Simultaneous measurements were carried out in order to eliminate the introduction of monthly variability in the harmonic constants. This was found to be necessary since monthly variability in harmonic constants actually exists, as shown in Foreman *et al.* (1995) and Kang *et al.* (1995). Automatic water level recorders with the same kind of paroscientific sensors were deployed at 5 stations (T1-T5). The quality of observed data was carefully checked by plotting and visual inspection, and in general the data quality was quite satisfactory. Water level data were sampled every 10-minutes and the non-tidal high frequency components were filtered out to yield hourly data. The time series of about one month were then analysed using a standard least square technique (Murray 1963; Foreman 1977). For a month-long data analysis 8 related components as well as 27 major components were included, with Mokpo being a tidal station of permanent reference.

One point to note here is that even though we allow for the possibility of over (or under) corrections by nodal correction, as noted by Godin and Gutierrez (1986), we analyzed the monthly data with nodal correction, in order to obtain harmonic constants reflecting these nodal effects. This was done because nodal corrections do not influence the spatial trend of variability among monthly harmonic constants from several locations provided that the effect is treated uniformly for monthly analyses. A detailed description of harmonic analyses of monthly tidal data was made in Kang *et al.* (1995).

Characteristics of principal tidal components

The results of the analyses at 5 stations for the major components (M_2, S_2, N_2, K_1, O_1) are listed in Table 2.

When comparing M_2 harmonic constants in 1992 with those in 1986, it is seen that the 1992 amplitude (phase lag) values for T1, T3 and T5, that is, 117.1 cm (22.1°), 109.1 cm (15.4°), and 114.1 cm (332.6°) are more or less similar to 1986 values at 86T1, 86T2 and 86T3, of 115.3 cm (24.6°), 111.9 cm (17.9°) and 114.4 cm (331.2°). Notice that the pattern of decreased amplitude at T3 (86T2) is equal in both observations. In addition, the M_4 amplitude (phase lag) in 1992, 11.1 cm (198.1°), 2.9 cm (205.3°) and 7.9 cm (154.1°) also shows a more or less similar pattern to those of 11.5 cm (195.2°), 2.2 cm (228.7°) and 8.1 cm (146.2°) in 1986. Even though there is some difference in the absolute values, an abrupt change in the M_4 amplitude and phase lag is still found in both observations. The difference in harmonic values between 1992 and 1986

Table 2. Tidal harmonic constants for major components of data measured in 1992 along the Uldolmok waterway. The locations are shown in Fig. 1.

Station	M_2		S_2		N_2		K_1		O_1	
	am cm	ph deg	am cm	ph deg	am cm	ph deg	am cm	ph deg	am cm	ph deg
T1	117.1	22.1	39.9	66.0	23.1	358.7	30.0	243.9	21.3	213.6
T2	115.5	22.5	39.3	66.2	22.7	358.9	30.1	245.1	21.2	216.3
T3	109.1	15.4	37.6	58.0	21.8	352.4	29.7	244.6	20.5	217.4
T4	113.4	337.8	42.6	10.6	22.8	316.5	30.5	221.8	20.8	194.0
T5	114.1	332.6	43.7	5.8	23.1	313.7	30.2	220.3	20.3	189.9

may be related to the monthly variation of harmonic constants in the surrounding seas of Korean Peninsula as investigated by Kang *et al.* (1995) and Kang *et al.* (2002), in which the seasonal variability was shown in detail to be driven by seasonal stratification of the Yellow and East China Seas. This change in monthly harmonic values suggests that the contemporary data are necessary for investigating the spatial variation in the study area, as done in the present case. From both observations, such a consistency in the trend of spatial distribution of harmonic values, is also found in other constituents and this permits us to further investigate the tidal phenomena in the channel.

Based upon the results listed in Table 2, we proceed to examine the tidal characteristics of major constituents in some detail. Considering the phase lags of the M_2, it is clear that the tidal waves propagate from T5 to T1. Notice that the amplitudes of the semi-diurnal components are considerably smaller at station T3, located at the narrowest section of the waterway. In the case of the diurnal constituents, the decreases in amplitude of T3 are quite small, and the amplitude of K_1 observed in 1986 does not show the same pattern of amplitude decrease. It is quite interesting to see that the diurnal constituents do not show the same clear pattern of amplitude decrease as the semi-diurnal constituents, even though N_2, with smaller or nearly equal amplitude to the diurnal constituents, shows such a pattern.

Considering the phase lags of the constituents it is clear that the tidal waves propagate from T5 to T1. It is also shown that a large difference in phase lag occurs between T4 and T2. The differences in phase lags between T2 and T4 for M_2, S_2, N_2, K_1 and O_1 are 44.7°, 55.6°, 42.4°, 23.3° and 22.3, respectively. It is noticeable that, in spite of the short distance between the stations (about 9 km), a big difference in phase lag occurs over the narrow part of the waterway. It seems that the tidal waves propagate faster than the usual speed of long wave propagation. It is also worth noting that the phase lag differences of semi-diurnal constituents are about two times as large as those of diurnal constituents. With relatively large amplitude of semi-diurnal constituents, this large phase lag will result in the stronger current speeds of semi-diurnal constituents over those of the diurnal constituents. Probably in the case of semi-diurnal constituents, it is likely that more potential energy is converted into kinetic energy through the narrow section, therefore inducing the smaller amplitude of semi-diurnal constituents. This will be further considered with numerical models.

Characteristics of shallow water tides

Shallow water tides are found in basins or rivers of shallow depth and they are generated as nonlinear interactions to external tidal oscillations (Godin 1972). The results of analyses at 5 stations for the shallow water tides are listed in Table 3.

In the case of overtide (M_4), the magnitude of amplitude along the waterway is in the order of 10 cm except for T3 located near the narrowest section of the channel, and it is quite interesting that the variation in amplitude along the waterway is not smooth. Furthermore, the amplitude distributions of compound tides MS_4, MN_4 also show the same trend as that of M_4. In the case of lower harmonics *MSf* and *MM*, the amplitudes at T3 are larger than those of other stations in contrast to higher harmonics. Such a significant amplitude variation of the shallow water constituents may be related to a non-linear phenomenon around the narrow part of the waterway.

The remarkable characteristic of quarter-diurnal tides or higher harmonics (M_4, MS_4 and MN_4) takes place in the phase lag distribution of the above components. The phase lag patterns of quarter-diurnal components show that the quarter-diurnal tidal waves propagate from a T5 to T1 direction, but discontinuous behavior or abrupt jumps in phase lags is found at T3, again strongly suggesting that some nonlinear process takes place around the narrowest

Table 3. Tidal harmonic constants of major overtides and compound tides by analysis of the data measured in 1992 along the Uldolmok channel, Korea.

Station	M_4		MS_4		MN_4		*MSf*		*MM*	
	am cm	ph deg	am cm	ph deg	am cm	ph deg	am cm	ph deg	am cm	ph deg
T1	11.1	198.1	9.8	262.4	4.6	152.3	1.2	68.2	3.2	150.7
T2	9.6	186.4	8.5	262.2	4.0	147.0	4.8	350.8	8.8	26.5
T3	2.9	205.3	3.7	294.9	0.6	157.3	13.1	190.6	10.9	233.0
T4	8.8	159.7	7.3	238.1	3.6	135.4	2.0	42.6	5.4	137.6
T5	7.9	154.0	6.9	224.8	3.3	120.9	0.4	186.0	4.1	147.6

part of the waterway. One point to keep in mind is that an external M_4 tidal wave propagating from T5 to T1 may exist, since its existence is expected to be possible by the propagation of a corresponding tidal wave around the southwestern end of the Korean Peninsula. The results of the two dimensional model for the M_4 tide in the Yellow and East China Seas (Kang *et al.* 1998; Lie 1996) support the interpretation that the external M_4 tide with 10 cm amplitude exists around the southwestern tip of the Korean Peninsula, as shown in Fig. 6a of Kang *et al.* (1998). In contrast to this external tidal wave, the locally-generated tidal wave is defined as one generated through a non-linear effect in the narrow part of the waterway. The phase lag and amplitude patterns of the quarter-diurnal components also suggest that the nonlinear process seems to be confined to the narrowest part, or the generated tidal wave appears to be strongly dissipated after generation. Therefore, the discontinuous behavior in amplitude and phase lag is probably not seen at T4 and T2.

In the case of lower harmonics, it is shown that the amplitude distributions of *MSf* and *MM* differ from those of M_4, MS_4 and MN_4. Relative high amplitudes appear at station T3 near the narrowest section of the waterway. This again implies that the external tidal waves from both boundary sides (T1,T5) are relatively weak and probably there is a source of energy for lower harmonics around the narrowest section of the waterway. Considering the amplitudes at T2 and T4 are larger than those at T1 and T5, the influence of generated lower harmonics seems to reach a little farther than those of higher harmonics.

For the sake of interpreting these findings, a hypothesis is proposed, in which the observed tidal phenomena in higher and lower harmonics result from the superposition of the co-oscillating (or external tide) from both the open boundaries of the channel and generated (internal) tides in the channel. Model experiments with such a hypothesis were carried out for the examination of the M_4 tide in the English Channel by Pingree and Maddock (1978). Inclusion of the generated wave to the hypothesis looks plausible, since the nonlinearity around the narrow channel will be large due to the existence of powerful and fast currents and a large current gradient. Numerical experiments have been carried out in order to qualitatively investigate the expected nonlinear phenomena in some detail, which will be treated in the following section. Also in the discussion section a simple analysis is made of the advection term in the equation for motion in order to examine the non-linear effect in order to understand the basic nonlinear mechanism in the channel.

3. A Two-dimensional tidal modelling

In order to investigate the possible nonlinear tidal phenomenon, two dimensional tidal modeling has been carried out. The governing equations are the depth-averaged, two dimensional equations of shallow water waves, which can be alternatively represented in terms of mass flux as follows:

$$\frac{\partial \eta}{\partial t} + \frac{\partial U}{\partial x} + \frac{\partial V}{\partial y} = 0 \tag{1}$$

$$\frac{\partial U}{\partial t} + \frac{\partial}{\partial x}\left(\frac{U^2}{h}\right) + \frac{\partial}{\partial y}\left(\frac{UV}{h}\right) = -gh\frac{\partial \eta}{\partial x} + fV - \frac{K_b}{h}\sqrt{U^2+V^2}\,U + F_x \tag{2}$$

$$\frac{\partial V}{\partial t} + \frac{\partial}{\partial x}\left(\frac{UV}{h}\right) + \frac{\partial}{\partial y}\left(\frac{V^2}{h}\right) = -gh\frac{\partial \eta}{\partial y} - fU - \frac{K_b}{h}\sqrt{U^2+V^2}\,V + F_y \tag{3}$$

where (x, y) is (east-west, north-south) direction coordinates, h total water depth, η surface elevation, U volume transport in x, V volume transport in y, f Coriolis parameter, $K_b = g/C^2$, g gravity acceleration, and C=Chezy coefficient. The full set of non-linear equations is solved with an ADI finite difference scheme (Kang 1991; Kang *et al.* 1998), which displays a second order accuracy in space and time. The characteristics of the numerical scheme are the same as the S21 scheme and described in detail by Abbott *et al.* (1981).

The momentum diffusion term was considered in terms of a subgrid-scale modelling technique, since momentum diffusion induced from the subgrid term is often larger than the dispersion effect (Elder, 1959) obtained from depth averaging of three dimensional motion. All of the motions induced by small-scale processes not directly resolved by a model grid (subgrid-scale) are parameterized in terms of horizontal diffusion processes. The terms F_x and F_y represent these unresolved processes and can be written as

$$F_x = \frac{\partial}{\partial x}\left(2A_M\frac{\partial u}{\partial x}\right) + \frac{\partial}{\partial y}\left\{A_M\left(\frac{\partial u}{\partial y} + \frac{\partial v}{\partial x}\right)\right\} \tag{4a}$$

$$F_y = \frac{\partial}{\partial y}\left(2A_M\frac{\partial v}{\partial y}\right) + \frac{\partial}{\partial x}\left\{A_M\left(\frac{\partial u}{\partial y} + \frac{\partial v}{\partial x}\right)\right\} \tag{4b}$$

where, with constant C_s and velocity component (u, v),

$$A_M = C_s \Delta x \Delta y \left[\left(\frac{\partial u}{\partial x} \right)^2 + \left(\frac{\partial v}{\partial x} + \frac{\partial u}{\partial y} \right)^2 / 2 + \left(\frac{\partial v}{\partial y} \right)^2 \right]^{1/2} \quad (4c)$$

For the coefficient of subgrid scale stress we use the Smagorinsky (1963) diffusion idea. The effect of subgrid-scale stress (SGS) modelling is described in detail by Abbott and Basco (1989). In particular, the effect of SGS modelling in the present study was found to be effective in preventing the numerical instability from occurring during calculation, as the momentum diffusion term does.

The bottom friction term has been expressed as a quadratic friction form following the general applicability of the quadratic friction law for semi-diurnal tide modelling (Pingree and Griffiths 1987). The Chezy coefficient was chosen for several values such as

$$C = 59.191 \quad \text{and} \quad 44.294 \ \text{m}^{1/2}/\text{s} \quad (5a)$$

These values lead to the friction coefficients, respectively,

$$K_b = 0.0028 \quad \text{and} \quad 0.0050 \quad (5b)$$

A relatively large coefficient was chosen to reflect the strong dissipation in the narrow channel and the damping effect of other constituents to the M_2 tide. Due to the relatively small range of water depth, a constant bottom friction coefficient was used instead of a depth-dependent form as used in Kang *et al.* (1998). The results with different frictions are more or less similar to each other, giving the same trend in results and major results presented for $K_b = 0.005$. With an artificially high bottom friction nearly locked is the flow for the tidal flat area, where datum depth is less than 0 m.

Computations

The present model domain consists of a 262(13.1

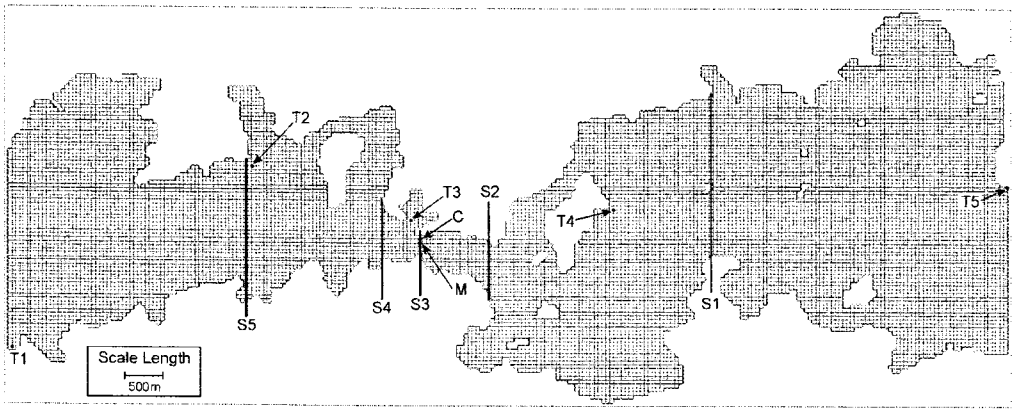

Fig. 3. Grid system for the modelled area. Tidal stations (T1-T5) for open boundary and verification along with central point M are illustrated in the figure. S1-S5 are the section for calculating M_2 energy flux. C is the point where Eulerian measurement is carried out in 2002.

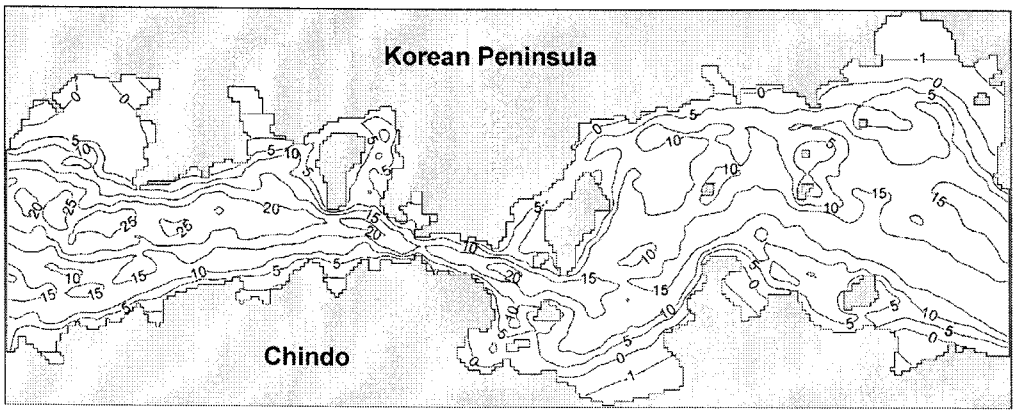

Fig. 4. Depth contour of the model area (unit: m).

km) × 103(5.2 km) grid with T1 and T5 being two open boundaries. The grid interval is 50 meters. The narrowest section of the channel consists of 5 grid cells, as shown in Fig. 3. Model depths are generally less than 30 m or so, along with some tidal flat regions, as seen in Fig. 4. The time step used is 5.45825 seconds, and the Courant number C_r, defined as

$$C_r = \frac{\Delta t\sqrt{g(h+\eta)}}{\Delta x}, \tag{6}$$

reaches to about 1.9 for the deep region of $h + \eta = 32.1$ m. This small Courant number was chosen to maintain accuracy in the rather complicated geography. A Coriolis parameter was calculated for the latitude of $\phi = 34°34'$N, based upon the f-plane assumption.

The initial and boundary conditions required for the solution of the equations (1) to (3) are described as follows. At $t = 0$, $U(x, y, t) = V(x, y, t) = 0$ are specified at all points. Boundary conditions for the tidal model consist of an absence of flow to the coast and specified elevations along the open boundaries. The open boundaries consist of two sections encompassing T1 and T5. Along the open boundaries M_2 and M_4 constituents are considered in the some combination, with constant values along the open boundary point listed using the observed values listed in Tables 2 and 3. The open boundary elevations are prescribed for the two constituents according to the expressions:

$$\eta(t) = \sum f_j A_j \cos(\omega_j t - G_j + V_{o_j} + U_j) \tag{7}$$

where f_j and U_j are the astronomical amplitude and phase corrections and Vo_j is the astronomical argument related to Greenwich. In this study f_j was set at 1.0 and $V_{oj} + U_j$ to zero, as these are reasonable approximations for M_2 and M_4.

Even though shallow water constituents are not included in the area of boundary forcing, the nonlinear terms in the governing equations generate the higher harmonics such as the M_4 constituent as well as the residual surface or tide-induced sea level disturbance. This result without M_4 boundary forcing could be compared with the results with M_4 boundary forcing.

In this study, the Smagorinsky eddy viscosity model was extended to the two-dimensional free surface flow model, and the empirical constant C_s of equation (4c),

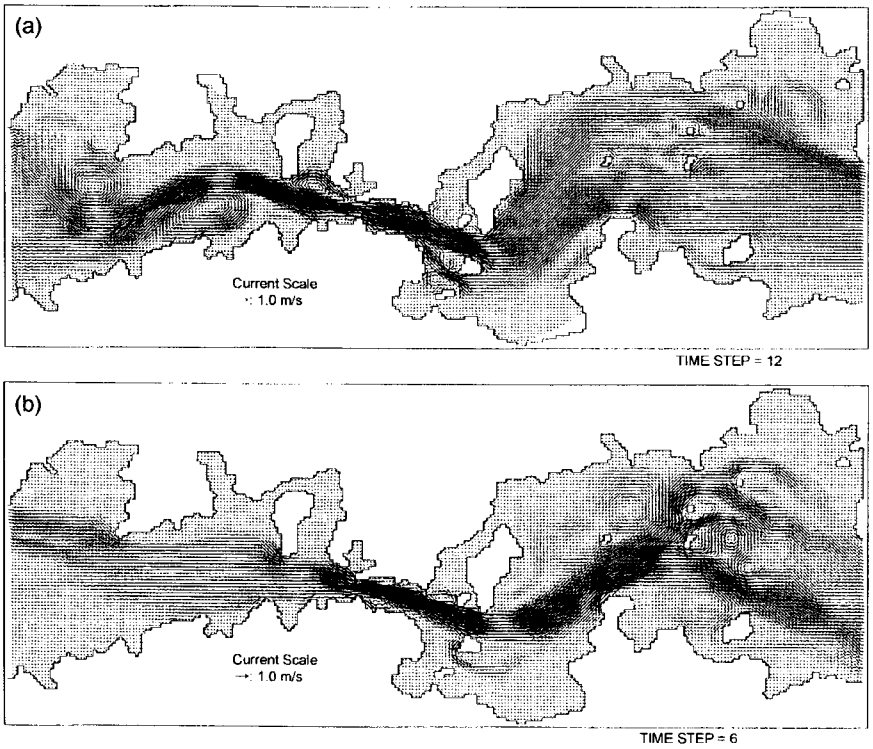

Fig. 5. (a) Computed flood current during mean tide (2.5 hr after low water), (b) Computed ebb current during mean tide (2.5 hr after high water).

dependent only on Kolmogorov's universal constant, will differ from the values of C_s-0.2 in the three dimensional studies, established by Deardorff (1970) and others. The constant for the Smagorinsky formula is chosen as $C_s = 0.38$ in the present study, which is a little larger than the value used by Lilly (1967) and Deardorff (1971) for the three dimensional study.

After an initial spin-up, one M_2 cycle run was carried out. The computed time series data are subject to the data analysis to calculate amplitudes and phases of the M_2 and M_4 constituents along with residual surface.

Current features

The computed flood and ebb current fields are shown in Fig. 5a and 5b, respectively. During a flood tide, the tidal current flows from the right to the left boundary, and vise versa during an ebb tide. It is shown that the tidal current moves like a jet stream along the channel. During a flood, the two eddies are seen to be formed in the left domain of the narrowest section, and the large eddy tends to move downstream as time passes. The axis pattern of the flow jet in Fig. 5a seems to imply that the major axis is controled by the strong large eddy. During ebb flows, the eddies are seen to form behind the small islands in the right section of the channel. Comparison of the eddies in Fig. 5b and the eddies computed one hour after (not shown here) shows that the time varying pattern of eddies behind the small islands is remarkable. The example of the time varying pattern of eddies behind the headland has been shown in research work by Geyer and Signell (1990; 1991) and Signell and Geyer (1991). The formation of eddies is thought to be due to the strong current shear behind the island or headland type of geography in the present case. The detailed verification for the eddy structures using instruments such as an ADCP has not been attempted yet, since the present study is focused on the nonlinear tidal dynamics in the strong current environments. Therefore, the verification for the performance of the present model is made in terms of the comparison between both the observed and computed harmonic values of M_2 and M_4.

Results and energy flux calculation for the M_2

The numerical experiment for the M_2 tide was carried out for the four combinations with/without the convection term, and with M_2 or $(M_2 + M_4)$ boundary forcing. The computation was first carried out with imposing one constituent M_2 at both open boundaries with/without the convection term. These are for investigating the pure generation effect of the M_4 pressure that occures near the M_2 boundary according to the existence or non-existence of a convection term. Next, experiments were carried out by imposing the $(M_2 + M_4)$ at both the boundaries with or without advection term, which could be used to the regeneration effect of the M_2 tide through M_2 and M_4 interaction.

The observed and computed harmonic values of the M_2 tide for the 4 cases are given in Table 4 at the points of T2, T3, T4 and middle point (M) of the narrowest section, as marked in Fig. 3. The computed results are presented except for the tidal flat area. Fig. 8a shows the M_2 tidal chart for the M_2 input condition with advection and Fig. 6b for the $(M_2 + M_4)$ input condition with advection. The solid line denotes co-amplitude and the dotted the co-phase line. Results in both Figures reveal that the amplitudes become smaller toward the narrow section. Co-amplitude lines in Fig. 6a vary from 116 cm at the left boundary to 108 cm at the narrow part, and in Fig. 6b from 116 cm to 110 cm. With regard to the phase lag, the co-phase line is plotted every 10 degrees. Over the short distance appears a large phase lag difference from 340° to 20° in both results. This large phase lag difference over a short distance indicates that the tidal wave in the narrow section does not propagate at the usual gravity wave speed.

Table 4 also shows that the observed and computed amplitudes of the M_2 tide decrease toward the narrowest section in all experiments, with the results of all cases roughly coinciding with observations. Generally, the decrease in amplitude around the narrow region (T3 and M) is larger in the case of experiments without the advection terms. To interpret this, it would be interesting to see how large the current speeds are for the cases with and without convection terms.

Co-speed charts of the x component of M_2 tidal currents are presented in Fig. 7a and 7b for without and with convection terms, respectively. It is clearly seen that the speed in the result without convection terms is much stronger than the results with convection terms. The x component of currents at central channel M is about 4.1 m/s, while it reaches about 6.7 m/s for the results without the advection term. This is probably because the experiment without advection cannot generate lots of eddies and higher harmonics as well as a change in the residual surface to be shown later. This results in much less energy dissipation than the experiments with advection. The x component of calculated current at C (Fig. 3) is 3.9 m/s, which is in quite good agreement with the observed depth-mean tidal speed of 3.3 m/s (MOMAF 2002).

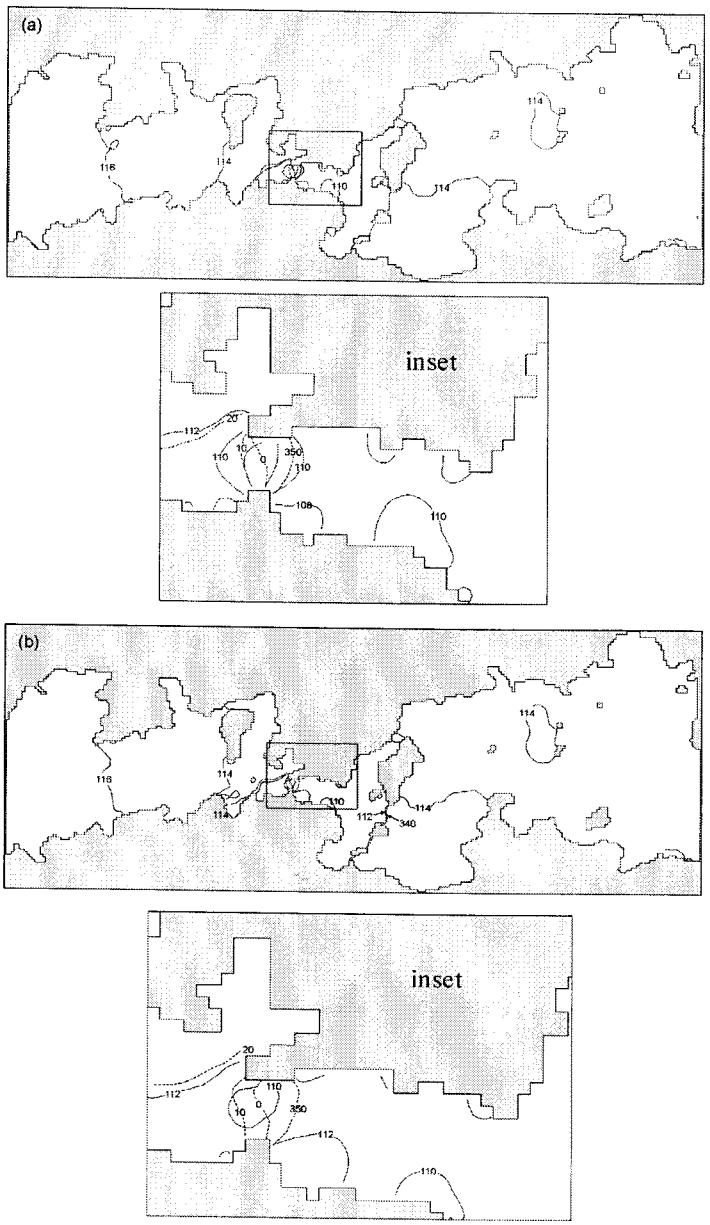

Fig. 6. Computed M_2 tidal chart for (a) M_2 forcing and (b) ($M_2 + M_4$) forcing. Unit of amplitude (solid line) is cm and phase lag (dotted line) degree. Results for narrow channel region is also given in inset.

Table 4. Computed results of the M_2 tide with different forcing constituents at open boundary (FCOB) with convection terms included(Y) or excluded(N).

FCOB	Convection terms	T2		T3		Mid point(M)		T4	
		am (cm)	ph (deg)	am (cm)	ph (deg)	am (cm)	ph (deg)	am (cm)	ph (deg)
M_2	N	113.5	20.5	107.5	13.5	106.2	5.8	113.4	338.6
	Y	115.0	22.2	112.2	21.2	107.2	0.8	114.5	336.0
$M_2 + M_4$	N	113.5	20.5	107.5	13.5	106.1	5.9	113.4	338.6
	Y	115.1	22.2	112.7	21.0	109.0	0.6	114.4	336.0
observed value		115.5	22.5	109.1	15.4	-	-	113.4	333.8

However, the relatively large inequality between observation and calculation at C, however, may be in part due to the neglect of frictional dissipation by other components or irrelevant representation of bottom friction by quadratic form. This seems to imply that some fundamental research for friction effect, along with increased consideration of tidal harmonics, is necessary in order to examine the tidal dynamics of the Uldolmok channel in the future, which is beyond the scope of the present study.

Meanwhile, the relatively small M_2 amplitude and high speed at the narrow region (T3 - M) for the non-advection case imply that more potential energy (than in the case of advection terms) is converted to kinetic energy. However, in the case of experiments with advection terms, the M_2 amplitude at M still decreases to a great extent. This also implies that the potential energy is converted to kinetic energy at the narrowest section, inducing the strong current speed there.

It is also worth noting that there exists a difference in the M_2 amplitude between Fig. 6a and 6b with the different boundary forcing. A careful look at the co-amplitude lines of Fig. 6 reveals some difference around the narrow section: e.g., co-amplitude line of 108 cm is not shown in Fig. 6b. This implies that the non-linear interaction between M_2 and M_4 play a role in regenerating M_2. An analysis of advection terms for the possibility of the M_2 regeneration has been made in the discussion section.

The energy flux over the five sections (S1-S5) of the channel shown in Fig. 3 have been calculated in order to estimate the power transfer through the channel and to investigate the energy balance along the channel. The vertically integrated energy flux (Foreman *et al.* 1995) is given by

$$\bar{F} = (H+\eta)\rho\left(\frac{1}{2}|\bar{u}|^2 + g\eta\right)\bar{u} \tag{8}$$

where $\rho(=1025\ \mathrm{kg/m^3})$ is a representative seawater density and H is the mean water depth. Since several contributions such as residual, M_4 and M_2 tides are expected even in an experiment with only M_2 boundary forcing with convection term, the mean M_2 energy flux over a cycle of tidal harmonics could be better obtained if it were based upon harmonic values rather than u, η values. If the elevation amplitude of a constituent is Z and its phase ϕ_z, and the east(west) velocity amplitude and phase lag are $\hat{U}(\hat{V})$ and $\phi_u(\phi_v)$, then x component F_x of mean energy flux over a period (T) of the constituent is

$$\begin{aligned}
F_x &= \frac{1}{T}\int_0^T (H+\eta)\rho\left(\frac{1}{2}|\bar{u}|^2 + g\eta\right)u_x dt \\
&= \frac{1}{T}\int_0^T \left\{\frac{1}{2}\rho H|\bar{u}|^2 u_x + \rho g H\eta u_x + \frac{1}{2}\rho\eta|\bar{u}|^2 u_x + \rho g\eta^2 u_x\right\} dt \\
&= \frac{1}{2}\rho g H\hat{U}Z\cos(\phi_z-\phi_u) + \frac{3}{16}\rho Z\hat{U}^3\cos(\phi_z-\phi_u) \\
&\quad + \frac{1}{16}\rho Z\hat{U}\hat{V}^2\cos(\phi_z+\phi_u-2\phi_v) + \frac{1}{8}\rho Z\hat{U}\hat{V}^2\cos(\phi_z-\phi_u)
\end{aligned} \tag{9}$$

The term $\frac{1}{2}\rho g H U Z\cos(\phi_z - \phi_u)$ is due to the potential energy flux, as is also shown by Ye and Robinson (1983), and the other terms are due to kinetic energy flux. Using the above relations the mean energy flux over a cycle of the M_2 tide is given in Table 5 for five sections.

Table 5 shows that the major energy flux (about 2/3) is from the eastern boundary (T5) and the energy flux decreases sharply in section 3. The ratios of kinetic energy flux (KEF) to total energy flux (TEF) are 0.2, 0.7, 3.7, 0.6 and 0.0%, which are quite small compared with the potential energy contribution. However, the ratio 3.7% at the narrowest section 3 are relatively large, indicating that more energy at section 3 than at others is transported in terms of kinetic energy, possibly resulting in a decrease in the M_2 amplitude of elevation.

The directions of energy flux deserve special attention. The directions of energy flux in sections 1 and 2 are opposite to those of sections 4 and 5. The propagation of energy flux from both sections 1 and 5 toward the central channel could be plausible since both sections are linked to coastal oceans, as shown in Fig. 4. This means that energy fluxes are toward the narrow section and the energy amounting to the difference in energy flux between sections 2 and 4 is consumed in the area surrounded by sections 2 and 4, or the energy convergence occurs there. The consumed energy reaches to 4.701×10^7 joule which is

Table 5. Average M_2 tidal energy flux($\times 10^7$ joule/s) across the five sections shown in Fig. 5, for M_2 boundary forcing with convection terms included. Energy flux(TEF) consists of potential energy flux(PEF) plus kinetic energy flux(KEF).

Section number	PEF	KEF	TEF
1	−4.206	−0.009	−4.215
2	−2.935	−0.022	−2.956
3	−0.800	−0.031	−0.830
4	1.734	0.011	1.745
5	2.093	0.001	2.094

about 75% of the energy flux difference between sections 1 and 5.

In order to estimate the energy dissipation contribution from bottom friction, the tidal dissipation has been calculated using time series data reproduced by harmonic constants, since integration of the bottom friction term is not easy. Following Glorioso and Simpson (1994), the mean rate of tidal energy dissipation per unit area due to bottom friction can be estimated by the expression

$$E_d(i,j)=C_d\rho N^{-1}\sum[u^2(i,j)+v^2(i,j)]^{3/2} \quad (10)$$

where velocity components $(u(i,j), v(i,j))$ are values at the center of each grid and N an interation number. The energy dissipation was integrated over the area between sections S2 and S4 in Fig. 3. The average dissipation of tidal power over the domain is 1.772×10^7 joules/s. This is about 38% of the total energy expected to be consumed there. An energy flux of 2.929×10^7 joules/s, roughly equal to the energy flux from the eastern boundary still needs to be explained.

The convergence of the M_2 tide around the narrow section implies quite complicated phenomena. Regarding the M_2 energy consumption, it is likely that this consumption is due to dissipation and/or energy use in relation to other dynamical processes such as generation of the M_4 tide and

Table 6. Computed results of the M_4 tide with different forcing constituents at open boundary (FCOB) with convections included(Y) or excluded(N).

FCOB	Convection terms	T2		T3		Mid point(M)		T4	
		am (cm)	ph (deg)	am (cm)	ph (deg)	am (cm)	ph (deg)	am (cm)	ph (deg)
M_2	N	0.3	205.9	0.9	201.7	1.2	200.8	0.4	195.3
	Y	0.8	6.7	6.2	359.1	23.2	1.0	0.6	333.2
M_2+M_4	N	11.1	189.5	11.0	186.8	10.8	183.0	8.8	161.3
	Y	10.1	190.6	5.0	204.2	13.5	4.0	7.8	157.2
observed value		9.6	186.4	2.9	205.3	-	-	8.8	159.7

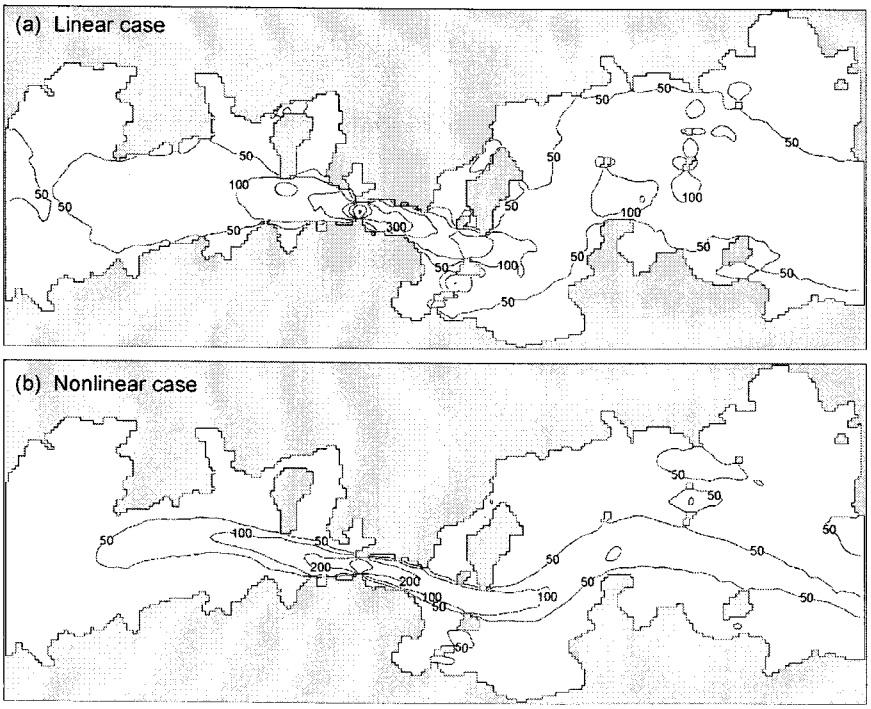

Fig. 7. Co-amplitude line of x component (cm/s) of the M_2 tidal current by forcing (a) without convection term and (b) with convection term.

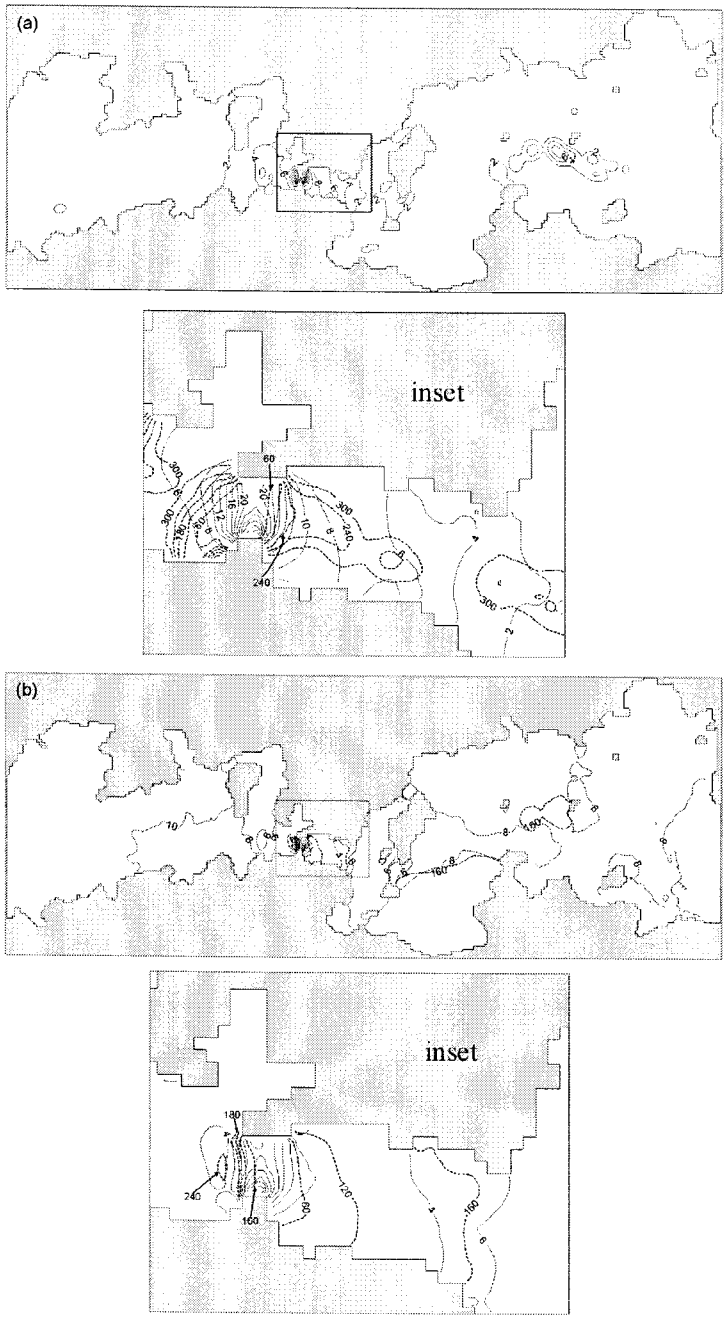

Fig. 8. Computed M_4 tidal chart for (a) M_2 forcing and (b) (M_2+ M_4) forcing.

depressing of the residual surface in the area. These will be described in the following sections.

Results for the M_4

The M_4 contributions in the channel are investigated for the cases with/without convection terms in the governing equations, and with/without M_4 in the boundary forcing. In the case of the English Channel, Pingree and Maddock (1978) calculated the M_4 contribution from the individual generating term in governing equations such as friction, advection and non-linear continuity as well as the contribution due to input at open boundaries.

The results for the higher harmonics M_4 in terms of various combinations of experimental cases are shown in Table 6 and Fig. 8a and 8b. Fig. 8a shows the M_4 tidal chart for only the M_2 input condition, and Fig. 8b

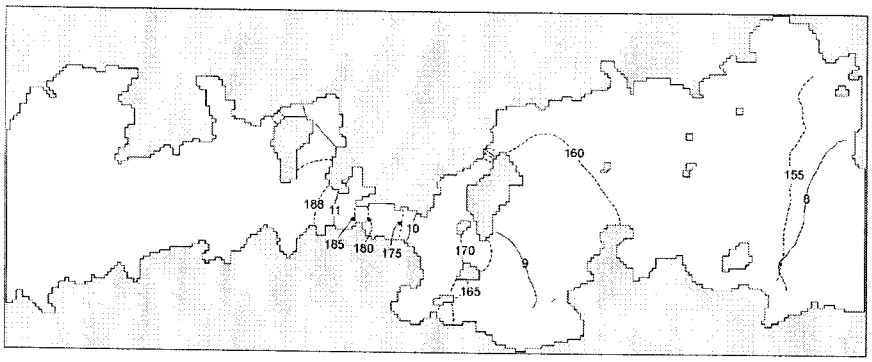

Fig. 9. M_4 tidal chart by (M_2+ M_4) forcing without convection term.

represents the M_4 tidal chart for (M_2 + M_4) input condition. Fig. 8a shows that the amplitudes are less than 2 cm for the most part except for the region around the narrow region. The amplitude of M_4 around the narrowest section is shown to be very large, indicating that the M_4 tide is strongly generated around the narrowest section. In the subset of Fig. 8a, the detailed tidal chart is presented with a dotted co-phase line. It is clearly seen that the strongest generation of the M_4 tide occurs around the narrowest section where strong current and large current shear occur, as shown in Fig. 7. It is interesting to note that the phase lag around the narrowest section is mostly 0°-60°, showing a smooth variation there, while a relatively sharp gradient occurs outside. However, Fig. 8b shows that the amplitude magnitudes in the domain are about 8-10 cm outside the narrow region. It is clear that this large amplitude outside the narrow section is due to the effect from the external tide propagating from the open boundaries. In the subset of Fig. 8b, it is seen that the amplitude tends to decrease up to about 4 cm, and increases to a large value around the central region. The phase lag also shows some distortion for this case with (M_2 + M_4) forcing, compared with the result with M_2 forcing.

The results of the 4 experiments are described in some detail in terms of comparison between observations and model results. In Table 6, the computed M_4 harmonic constants for different cases of open boundary forcing as well as for inclusion of convection terms are listed at 4 points along the channel. Again Table 6 indicates that the computed results, for the case with (M_2 + M_4) boundary forcing as well as with convection terms, show a reasonable agreement with the observed values. The computed amplitudes for the case with M_2 forcing and without convection are less than 1.2 cm at all stations while the amplitudes at T3 and M are 6.2 and 23.2 cm for cases with M_2 boundary forcing and convection terms considered. This indicates that the convection terms play a critical role in the internal generation of the M_4 tide. This is comparable to the results of Pingree and Maddock (1978). As mentioned, the locally concentrated high M_4 amplitudes both at T3 and M (see Fig. 8a) indicates that the non-linear internal generation of the M_4 tide is focused around the narrowest section of the channel. The M_4 characteristics at T3 with M_2 forcing and advection suggest that this station is under the influence of the strong generation at the narrowest section. However, the results of this case still do not coincide with that of observations, since the computed amplitudes at T2 and T4 are much less than the observed amplitudes, while the computed amplitude at T3 is much larger than the observed value. Furthermore, the difference in phase lag attains a level of more or less 180°.

Experiments with (M_2 + M_4) boundary forcing show quite different results in terms of amplitude distribution, compared with the results with M_2 boundary forcing. Fig. 9 represents the M_4 tidal chart with (M_2 + M_4) forcing and without convection terms. The amplitudes are more than 8 cm in the whole region, and the amplitudes at four points are larger than 8.8 cm, as listed in Table 6. Considering phase lag, it is seen that the external M_4 tidal wave propagates from eastern to western boundaries without any abrupt change in the phase lag. The amplitude and phase lag in this case agrees with those observed except for T3. This means that the M_4 tidal characteristics at T2 and T4, where the size of the generated amplitude is less than 1.0 cm, is governed mainly by M_4 boundary forcing. Also notice that the computed phase lag (186.8°) at T3 is nearly out of phase with the generated phase lag (359.1°) based on the result obtained as a result of forcing and convection terms.

The M_4 tidal chart with (M_2 + M_4) forcing and the advection term is compared with the results with

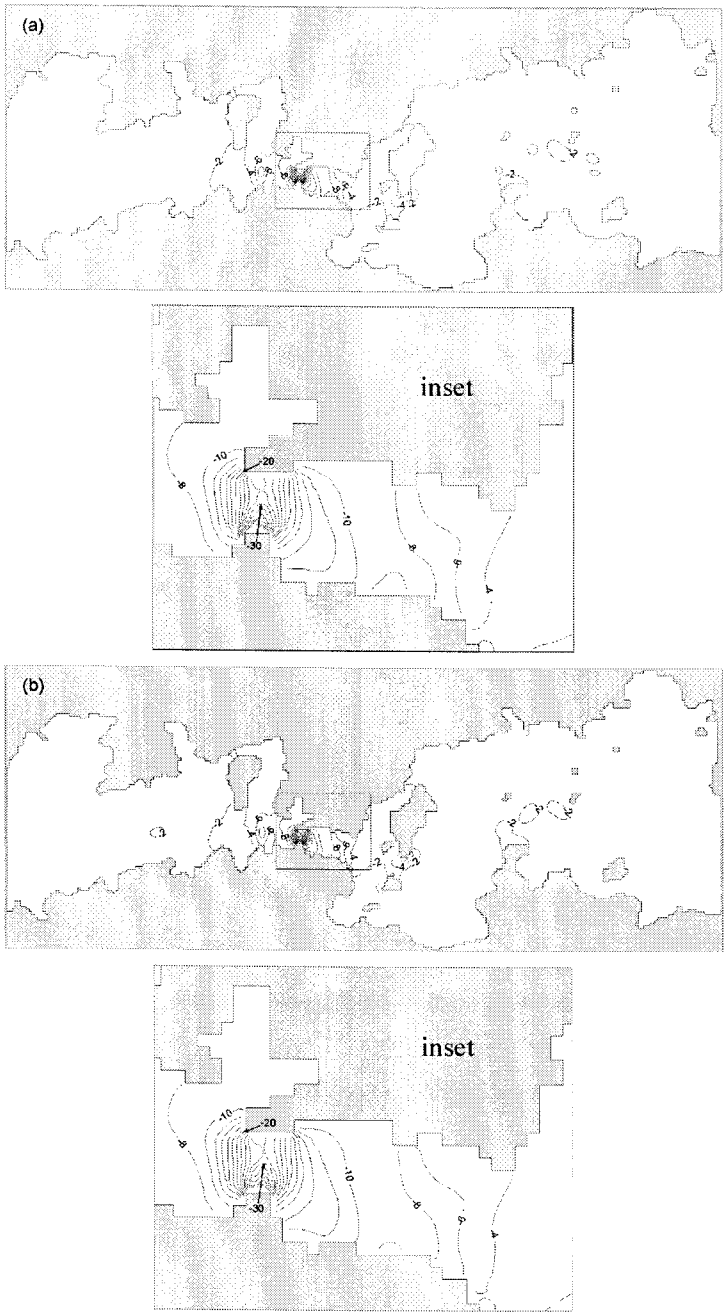

Fig. 10. Computed co-residual surface (or mean sea level) (cm) for (a) M_2 and (b) (M_2+M_4) boundary forcing.

($M_2 + M_4$) forcing and without the advection term. The amplitude and phase lag differences in both results are clear especially around the narrow section. The phase lag in this case does not show an abrupt change around the narrow region where strong M_4 generation occurs and the distorted pattern in amplitude from the generated one is also seen. Explicit comparison (Table 6) between the computed result and the observation shows that the computed amplitudes and phase lags at T2, T3 and T4 are in good agreement with the observations. The computed amplitude at T3 shows an abrupt decrease as well as a discontinuous phase lag, a trend that also appears in observed values at T3.

These results indicate that the amplitude and phase lag in the channel are determined by the superposition of the internally generated M_4 and the M_4 propagated from the

open boundaries. More precisely, at T2 and T4 or in the region apart from the narrowest section, the part due to boundary forcing plays a much larger role in determining the amplitudes than the contribution through generation. However, at point M, the generated amplitude is much larger than the amplitudes induced from boundary forcing. This large amplitude with nearly no change from the generated value in the phase lag, in the results of convection and (M_2+M_4) forcing, suggest that the M_4 at M is mainly determined by the non-linear generation effect. Meanwhile, at T3 the generated amplitude of the M_4 at T3 (6.2 cm) is comparable to the amplitude 11.0 cm obtained in the case of non-convection and (M_2+M_4) boundary forcing. This implies that M_4 at T3 is not determined wholly either by the external part or the generated part.

In order to quantitatively investigate the superposition of each contribution at T3, we do simple complex summation of both parts. The result of M_2 forcing and convection is considered the case for pure generation effect of the M_4, while (M_2+M_4) the result with and without convection can be counted as a constituent determined by boundary forcing, since other non-linear generation effects such as friction is expected to be minor. Summation from both contributions at T3 yields

$$6.2e^{359.1i}+11.0e^{186.8i}=4.9e^{196.5i} \tag{11}$$

Amplitude of 4.9 cm and phase lag of 196.5° nearly reach the observed values at T3, 2.9 cm and 205.3°. Interestingly, this also explains the discontinuity in the phase lag. Therefore, from the results it can be said that the abrupt decrease in M_4 amplitude at T3 is due to the locally generated component, being nearly out of phase with the propagated component arising from boundary forcing. Similarly, the propagation of the M_4 tidal waves from the one open boundary (T5) to the other boundary (T1) is distorted, as shown in Fig. 8b, by the existence of an out-of-phase M_4 tide around the narrowest section of the channel, which is generated by strong M_2-M_2 non-linear interaction. This distortion appears as a discontinuity of the M_4 phase lag in T3 and M where the magnitudes of the generated amplitude are little less or much larger than the propagated one from open boundaries.

The above experiments have shown that the generation of the higher harmonic M_4 is quite strong around the narrowest section of the channel and it is expected that the other shallow water constituents such as MS_4 and MN_4, whose characteristics are dominantly governed by the M_2 tide, could be explained by similar physical processes as for the M_4 tide.

Results for mean sea level

Tide-induced residual surfaces or mean sea levels are often presented in model works (Pingree and Griffiths 1978; Foreman *et al.* 1995; Gloriosp and Simpson 1994). However, a comparison between observed and computed results is rarely made probably due to the lack of observed data and the complexities involved. Due to the geographical and coastal characteristics of Uldolmok waterway, the observation of tidal levelling became possible, as seen in Fig. 1 and 2. This enables us to attempt to verify the computed residual surface against observations.

The computed result for the residual sea level (tide-induced mean sea level) is shown in Fig. 10a for M_2 boundary forcing and Fig. 10b for (M_2+M_4) forcing with convection terms. (The results without the advection term are not presented due to its negligible order of magnitude less than 1.0 cm.) The detailed structures of the residual sea surface around the narrow region are presented in each subset of the figures. The difference between results for M_2 and (M_2+M_4) boundary forcings is nearly unnoticeable, since input boundary forcing of mean sea level was not included in either case. These figures illustrate that there is a clear trend of amplitude decreasing toward the narrow section, even though some local variabilities of the computed mean sea level are found around the corner area. The decrease of mean sea level at T3 is about 8.5 cm, which coincides with the magnitude of the observed mean sea level shown in Fig. 2 where the mean sea level at 86T2 is 10 cm lower than at 86T1 and 7 cm lower than at 86T3. The minimum decreasing of mean sea level is seen to reach up to 30 cm in the narrowest central section as illustrated in the figure.

This result demonstrates that the change in the local mean sea level is possible, and the prediction can be made with reasonable accuracy. The verification of the M_4 distribution reinforces the modelled variation for the mean sea level, since this variation can be explained in a similar manner to the M_4 variation, as discussed in the next section.

4. Discussions

The numerical model has shown that the advection term plays a critical role in generating the M_4 tide and depressing the mean sea level. In addition, an analytical consideration for the advection term is made in order to investigate qualitatively the generation effect of the M_4 tide, the tide-induced change in the mean sea level, and the regeneration of the M_2 tide through M_2 and M_4 interaction in the

channel. For simplicity, the channel is assumed to be a one-dimensional channel. The flow is assumed to consist of two tidal constituents with angular frequencies of ω_1 and ω_2 and current amplitudes of $u_1(x)$ and $u_2(x)$, and phase lags of θ_1 and θ_2. Then the flow is represented as follows.

$$u = u_1(x)\sin(\omega_1 t - \theta_1) + u_2(x)\sin(\omega_2 t - \theta_2) \quad (12)$$

The advection terms become

$$\begin{aligned}
u\frac{\partial u}{\partial x} &= \frac{1}{2}[u_1u_1'\{1-\cos(2\omega_1 t-2\theta_1)\}-u_1^2\theta_1'\sin(2\omega_1 t-2\theta_1)\\
&+u_2u_2'\{1-\cos(2\omega_2 t-2\theta_2)\}-u_2^2\theta_2'\sin(2\omega_2 t-2\theta_2)]\\
&-\frac{1}{2}u_1u_2'[\cos\{(\omega_1+\omega_2)t-(\theta_1+\theta_2)\}-\cos\{(\omega_1-\omega_2)t-(\theta_1-\theta_2)\}]\\
&-\frac{1}{2}u_1u_2\theta_2'[\sin\{(\omega_1+\omega_2)t-(\theta_1+\theta_2)\}+\sin\{(\omega_1-\omega_2)t-(\theta_1-\theta_2)\}]\\
&-\frac{1}{2}u_1'u_2[\cos\{(\omega_1+\omega_2)t-(\theta_1+\theta_2)\}-\cos\{(\omega_2-\omega_1)t-(\theta_1-\theta_2)\}]\\
&-\frac{1}{2}u_1u_2\theta_1'[\sin\{(\omega_1+\omega_2)t-(\theta_1+\theta_2)\}+\sin\{(\omega_2-\omega_1)t-(\theta_2-\theta_1)\}]
\end{aligned} \quad (13)$$

where primes in $u_{1,2}'$ and $\theta_{1,2}'$ denotes partial differentiation with respcect to x. Eq. (13) indicates that the advection term with input tidal forcing with two frequencies of ω_1 and ω_2 generates new tidal oscillations having the frequencies of $2\omega_1$, $2\omega_2$, $(\omega_1+\omega_2)$, $(\omega_1-\omega_2)$, and 0. The motion with 0 frequency denotes the variation of mean water level with spatially varying amplitude $\frac{1}{2}\{u_1(x)u_1'(x)+u_2(x)u_2'(x)\}$. This value explains the existence of the varying local mean sea level shown in Fig. 10. The strong current speed and large shear in the speed may explain the large amplitude of the mean sea level in the narrowest section of the channel.

If instead of two constituents only one constituent from the open boundary is given, that is, $u_2=0$, the advection term becomes

$$\begin{aligned}
u\frac{\partial u}{\partial x} &= \frac{1}{2}\{u_1u_1'-u_1u_1'\cos(2\omega_1 t-2\theta_1)-u_1^2\theta_1'(2\omega_1 t-2\theta_1)\}\\
&= \frac{1}{2}\left\{u_1u_1'-\sqrt{(u_1u_1')^2+(u_1^2\theta_1')^2}\sin(2\omega_1 t-2\theta_1+\alpha)\right\},\\
\tan\alpha &= \frac{u_1'}{u_1\theta_1'}
\end{aligned} \quad (14)$$

This means that additional constituents with frequencies of 0 and $2\omega_1$ are generated and the phase lag of generated motion is $(2\theta_1-\alpha)$. The motion with 0 frequency now induces the variation of mean water level with spatially varying amplitude of $\frac{1}{2}u_1(x)u_1'(x)$ and spatially varying M_4 amplitude of $\frac{1}{2}(u_1(x)u_1'(x)+u(x)_1^2\theta'(x)_1)$.

It is interesting to note that the spatial distribution of the amplitude of the residual surface (Fig. 10a) is actually more or less similar to that of the generated M_4 amplitude (Fig. 8a) in magnitude around the narrow section of the waterway. Considering the amplitude distribution of the residual surface is explained by $\frac{1}{2}u_1(x)u_1'(x)$, such a similarity could be explained in terms of the dominance of $u_1(x)u_1'(x)$ over $u(x)_1^2\theta'(x)_1$ in the generation of M_4. Additionally, as described in the results for the mean sea level, it is likely that the verification of the M_4 partly supports the modelled result of the mean sea level.

We proceed to estimate the generation of M_2 through M_2 and M_4 interaction. If $\omega_1 = M_2$ and $\omega_2 = M_4$ in eq. (13), the generated constituents from the advection term are 0, $M_4(=2\omega_1)$, $M_8(=2\omega_2)$, $M_6=(\omega_1+\omega_2)$, $M_2(=|\omega_1-\omega_2|)$. The regeneration of the M_2 by the non-linear interaction between M_2 and M_4 by the terms with frequency $|\omega_1-\omega_2|$ is natural and interesting. As shown in the model result of Table 4 and Fig. 8a and 8b, the magnitude of the M_2 tide appears differently depending upon whether M_2 or (M_2+M_4) is prescribed in the open boundary. Eventually, the new generation of the M_2 through M_2 and M_4 interaction may explain this M_2 variation.

5. Summary

In this study, shallow-water tides are described along the Uldolmok waterway, located on the southwestern tip of Korean Peninsula, where strong tidal flows up to more than 10 knots exist at the narrowest part. Harmonic analyses of the observed water levels reveal that there are rapid changes in the amplitudes and phase lags of shallow water constituents, M_4, MS_4, MN_4, MSf, MM at the station located near the narrowest part. The abrupt changes of harmonic constants of higher harmonics, M_4, MS_4 and MN_4 take place in a reverse pattern of amplitude distribution, compared with those of lower harmonics, MSf and MM. Also, it was observed that the amplitude of semi-diurnal constituents, M_2 and S_2, are obviously diminishing toward the narrowest part from both the open boundaries.

A non-linear two dimensional numerical model has shown that the directions of M_2 energy flux are toward the narrow section from both boundaries and about two thirds that of the incoming energy flux toward the region coming

from the eastern boundary. In particular, energy roughly equal to the energy flux from the eastern boundary (average of those in sections 1 and 2) is expected to be utilized for the mean sea level depressing and generating the M_4 tide there, since frictional damping does not account for the whole energy consumption. Also, the regeneration effect of the M_2 constituent through the interaction between the major M_2 forced from the boundaries and quarter-diurnal constituent M_4 was found to exist.

This study also demonstrates that the M_4 generation is very strong around the narrowest section of the channel, and the characteristics of the M_4 along the waterway are explained by the superposition of the external tidal oscillations from both boundaries and the internally generated oscillation through the advection effect. This superposition also explains the abrupt change of M_4 tide and discontinuity of phase lag around the narrow region. This process is expected to explain the discontinuity of the other higher harmonic constituents such as MS_4 and MN_4 governed mainly by the M_2 tide. The results for other shallow water constituents will be reported in the next stage.

In this paper, it is also shown that there is a clear trend for the mean sea level to decrease toward the narrow section, and this agrees well with observations. Furthermore, the verification of the M_4 distribution against observation reinforces the modelled variation in the mean sea level, since the amplitude distribution of the residual surface can be explained similarly to that of the M_4 tide.

Acknowledgements

We thank the technical staff of KORDI for their support in field observations, and Mikyung Kim for drafting the figures. Tidal levelling was designed and carried out by Prof. Sang-Ryong Lee, Pusan Nat'l Univ., during his career in KORDI and the basic idea for the nonlinear characteristic of tidal regime is hinted at by him and we thank him for providing the initial inspiration for this study. This work was partially funded by the Korea Ministry of Science and Technology through Grant PM18600 and PM19100.

References

Abbott, M.B., A. McCoWan, and I.R. Warren. 1981. Numerical modelling of free-surface flows and coastal waters. In : *Transport models for inland and coastal waters*, eds. by H.B. Fisher, Academic Press, New York.

Abbott, M.B. and D.R. Basco. 1989. Computational fluid dynamics : an introduction for engineers. John Wiley & Sons Inc., 425 p.

Deardorff, J.W. 1971. On the magnitude of the subgrid scale eddy coefficient. *J. Comp. Phys.*, 7, 120-133.

Elder, J.W. 1959. The dispersion of a marked fluid in a turbulent shear flow. *J. Fluid Mech.*, 5, 544-560.

Foreman, M.G.G. 1977. Manual for tidal heights analysis and prediction. Pacific marine science, report, 77-10, IOS, British Columbia, Canada.

Foreman, M.G.G., R.A. Walters, R.F. Henry, C.P. Keller, and A.G. Dolling. 1995. A tidal model for eastern Juan de Fuca Strait and the southern Strait of Georgia. *J. Geophys. Res.*, 100(C1), 721-740.

Geyer, W.R. and R.P. Signell. 1990. Measurements of tidal flow around a headland with a shipboard acoustic Doppler profiler. *J. Geophys. Res.*, 95, 3189-3197.

Geyer, W.R. and R.P. Signell. 1991. Measurements and modelling of the spatial structure of nonlinear tidal flow around a headland. p. 403-418. In: *Tidal Hydrodynamics*, ed. by B.B. Parker.

Glorioso, P.D. and J.H. Simpson. 1994 Numerical modelling of the M_2 tide on the northern Patagonian Shelf. *Conti. Shelf Res.*, 14(2/3), 267-278.

Godin, G. 1972. The analysis of tides. University of Toronto Press, Toronto. 264 p.

Godin, G. and G. Gutierrez. 1986. Non-linear effects in the tide of the Bay of Fundy. *Conti. Shelf Res.*, 5, 379-402.

Kang, S.K. 1991. Non-linear tidal modelling of the East China Sea, the Yellow Sea, and the East Sea. M. Sc. Thesis, H.H. 65, Int. Inst. for Hydra. and Env. Eng.(IHE) and Danish Hydraulic Institute.

Kang, S.K., J.Y. Chung, S.-R. Lee, and K.D. Yum. 1995. Seasonal variability in the M_2 tide in the seas adjacent to Korea, *Con. Shelf Res.*, 15(9), 1087-1113.

Kang, S.K., M.G.G. Foreman, H.J. Lies, J.H. Lee, J. Cherniawsky, and K.D. Yum. 2002. Two-layer tidal modeling of the Yellow and East China Seas with application to seasonal variability of the M_2 tide. *J. Geophys. Res.*, 107 (C3), 6-1-6-9.

Kang, S.K., S.R. Lee, and H.J. Lie. 1998. Fine grid tidal modelling of the Yellow and East China Seas. *Con. Shelf Res.*, 18, 739-772.

KORDI. 1986. Korea tidal power study-1986, Volume 1 Data, Report no. BSPI-00050-124-2, 299 p.

Lie, H.J. 1996. Ocean circulation and material flux of the East China Sea (third year) -Eastern East China Sea-. (In Korean and English abstract), BSPN 00278-901-1, 467 p.

Lilly, D.K. 1967. The representation of small scale turbulence in numerical simulation experiments. In : Proceedings of the IBM Scientific Computing Symposium on Environmental Sciences, IBM form No. 320-1951.

MOMAF. 2002. Development of utilization technique for ocean energy (II): Tide · Tidal current energy. (In Korean

and English abstract). BSPM 13200-1457-2. 337 p.

Murray, M.T. 1963. Tidal analysis with an electric digital computer. *Cashiers Oceanography*, 699-711.

Pingree, R.D. and D.K. Griffiths. 1978. Tidal fronts on the Shelf Seas around the British Isles. *J. Geophys. Res., Chapman Conference Issue*, 83, 4615-4622.

Pingree, R.D. and D.K. Griffiths. 1987. Tidal friction for semidiurnal tides. *Con. Shelf Res.*, 7, 1181-1209.

Pingree, R.D. and L. Maddock. 1978. The M_4 tide in the English Channel derived from a non-linear numerical model of the M_2 tide. *Deep-Sea Res.*, 25, 53-63.

Signell, R.P. and W.R. Geyer. 1991. Transient eddy formation around headlands. *J. Geophys. Res.* (in Press).

Smagorinsky, J.S. 1963. General circulation experiment with the primitive equations : I. the basic experiment. *Monthly Weather Review*, 91, 99-164.

Ye, A.L. and I.S. Robinson. 1983. Tidal dynamics in the South China Sea, Geophys. *J. R. Astr. Soc.*, 72, 691-707.

Received Feb. 15, 2003
Accepted Mar. 17, 2003